ChemComm

COMMUNICATION

View Article Online
View Journal

Cite this: DOI: 10.1039/d5cc03614c

Titanium surface nitriding by sodium amide in molten salts†

Tao Wang, *[a] Yiyu Wang,[b] Siyuan Gao,[a] Juntian Fan[a] and Sheng Dai [a]

Received 26th June 2025,
Accepted 25th July 2025

DOI: 10.1039/d5cc03614c

rsc.li/chemcomm

A crystalline titanium nitride (TiN) layer on titanium foil is achieved using sodium amide ($NaNH_2$) as a nitrogen source in LiCl–KCl molten salts. Nanoindentation testing revealed exceptional mechanical properties, with the nitrided surface achieving a hardness of approximately 20.6 GPa, representing more than a four-fold increase compared to the untreated titanium substrate.

The development of advanced nuclear reactor technologies demands materials capable of withstanding extreme operating conditions while maintaining structural integrity and chemical stability over extended service periods.[1] Among the critical challenges facing nuclear fuel systems is fuel-cladding chemical interaction (FCCI), a phenomenon that occurs at the fuel-cladding interface during irradiation and represents a primary performance limitation for metallic fuels in fast reactor systems.[2–4] FCCI involves complex interdiffusion processes between cladding constituent elements and fuel components or fission products, leading to the formation of intermetallic phases that can compromise cladding integrity and ultimately result in fuel failure.[5,6] This phenomenon typically occurs when fuel swells during irradiation and when buildup of fission products moves to the interface between the cladding and the fuel, reacting to form intermediate phases with poorer mechanical properties, effectively thinning the cladding material, and severely compromising the reliability of the cladding structure.[7]

Titanium nitride (TiN) is a highly promising material for mitigating FCCI in nuclear reactors due to its unique combination of properties.[8–10] It offers excellent corrosion and erosion resistance, chemical inertness, high melting point (2927 °C), and strong mechanical and electronic characteristics.[11–14] TiN has been widely used as a diffusion barrier in high-temperature applications, including in the integrated circuit industry, where thin TiN films prevent metal diffusion at elevated temperatures.[11] These properties are directly applicable to nuclear cladding, where diffusion barriers are essential for preventing migration of fission products. For example, Khatkhatay *et al.* confirmed TiN's effectiveness as a barrier to lanthanide fission products like cerium.[8] Their diffusion experiments showed that a 500 nm-thick TiN layer entirely blocked Ce diffusion into iron substrates at 600 °C, comparing to those uncoated samples.[8] These results highlight TiN's strong potential to enhance the performance and longevity of nuclear fuel cladding.

Traditional titanium nitriding methods include gas nitriding, plasma nitriding, and laser nitriding, each with advantages and drawbacks. Gas nitriding, the most common technique, diffuses nitrogen into titanium at 850–1050 °C for 10–50 hours using ammonia atmospheres.[15] It produces TiN/Ti_2N layers 1–5 μm thick with hardnesses of 900–1100 HV but requires long times, careful temperature control, and poses safety risks due to ammonia use. Plasma nitriding improves control and allows treatment of complex shapes by using reactive nitrogen plasma at 700–900 °C for 4–20 hours, yielding 1200–1800 HV hardness.[16,17] Laser nitriding uses focused lasers in nitrogen atmospheres to rapidly (under 0.1 hour) form TiN layers at 1200–1500 °C.[18,19] However, plasma and laser systems are complex and require careful optimization for uniformity, which are limited by high cost, equipment complexity, and risk of thermal damage to substrates. These limitations highlight the need for widely adaptable nitriding techniques tailored to achieve highly crystalline TiN cladding layers.

Herein, we report a surface nitriding strategy using sodium amide ($NaNH_2$) as a nitrogen source and molten LiCl–KCl as a flux media (Scheme 1). The $NaNH_2$-mediated nitridation involves several advantages over conventional ammonia-based processes. The solid-state nature of $NaNH_2$ eliminates the safety hazards associated with high-pressure ammonia gas systems while providing a controlled and localized nitrogen source.[20–22] In addition, the reaction produces highly crystalline products with improved mechanical properties compared to conventional coarse-grained materials. The molten-salt flux

[a] Chemical Sciences Division, Oak Ridge National Laboratory, Oak Ridge, TN 37831, USA. E-mail: wangt@ornl.gov
[b] Materials Science and Technology Division, Oak Ridge National Laboratory, Oak Ridge, TN 37831, USA

† Electronic supplementary information (ESI) available. See DOI: https://doi.org/10.1039/d5cc03614c

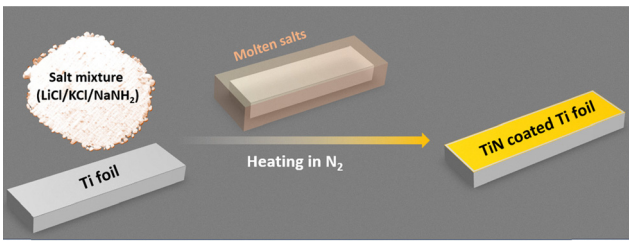

Scheme 1 Illustration of Ti surface nitriding process in molten salts.

media ensures intimate contact between the nitrogen source and the substrate surface, promoting uniform nitride layer formation even on complex geometries.[23,24] The integration of $NaNH_2$ with molten salt systems represents a further advancement that combines the benefits of low-temperature nitride formation with enhanced mass transport and reaction kinetics.

The LiCl–KCl eutectic composition (58 mol% LiCl, 42 mol% KCl) has a low melting point of 352 °C (Fig. S1, ESI†). The chloride-based molten salts provide chemical inertness toward titanium substrates and the ability to dissolve various nitrogen-containing compounds while maintaining a reducing environment that prevents competitive oxidation reactions. The most immediately apparent indication of successful titanium surface nitriding was the dramatic visual transformation of the titanium foil specimens following the molten salt treatment (Fig. 1a). The pristine titanium foil exhibited the characteristic bright metallic silver appearance typical of freshly cleaned titanium surfaces. After the 2 hour nitriding treatment at 900 °C in the $NaNH_2$-containing LiCl–KCl molten salt, the specimens underwent a striking color change from silver to a distinctive golden hue. The TiN coated Ti foil was named as Ti–TiN. This color transformation is characteristic of titanium nitride formation and has been consistently observed in various titanium nitriding processes reported in the literature.[25] The golden coloration arises from the optical properties of the TiN phase, which exhibits metallic luster with selective absorption and reflection characteristics that produce the distinctive golden appearance. The uniformity of the color change across the entire specimen surface provided initial evidence of successful and homogeneous nitride layer formation, suggesting that the molten salt medium effectively facilitated uniform nitrogen diffusion and reaction across the titanium surface.

X-ray diffraction (XRD) analysis provided definitive confirmation of titanium nitride (TiN) formation and enabled detailed characterization of the nitrided layer's crystallographic structure. Fig. 1b compares XRD patterns from the pristine titanium foil and the nitrided Ti–TiN specimen. The untreated titanium exhibited diffraction peaks at 2θ values of 35.1°, 38.4°, 40.2°, 53.0°, 62.9°, and 70.7°, corresponding to the (100), (002), (101), (102), (110), and (103) planes of hexagonal close-packed (hcp) α-titanium. These peaks matched well with the ICDD reference pattern for titanium (PDF #44-1294), confirming the purity and crystalline quality of the starting material. In contrast, Ti–TiN exhibited additional peaks at 36.7°, 42.6°, 61.8°, 74.1°, and 78.0°, corresponding to the (111), (200), (220), (311), and (222) planes of face-centered cubic (fcc) TiN. These matched the ICDD TiN reference pattern (PDF #38-1420), confirming successful nitride formation.

Scanning electron microscopy (SEM) analysis provided critical insights into the surface morphology and microstructure of the TiN layer in Ti–TiN. As shown in Fig. 2a, the low-magnification SEM image of pristine Ti foil reveals micron-sized scratches on surface. After nitriding, a uniform layer of submicron particles could be identified on the scratch surface (Fig. 2b). The surface closely followed the contours of the pristine Ti foil, suggesting a conformal growth mechanism that maintained substrate geometry while forming the TiN layer. At higher magnification (Fig. 2d), SEM images revealed densely packed submicron crystalline grains, consistent with the sharp diffraction peaks in X-ray diffraction (Fig. 1b). Clear grain boundaries and the absence of amorphous phases in the high-resolution images indicate high crystallographic quality, supporting robust mechanical performance. Notably, the fine-grained nanocrystalline structure observed here offers a distinct advantage over conventional nitriding methods, which typically produce coarser grains in the 1–10 μm range. The refined microstructure is expected to enhance hardness through the

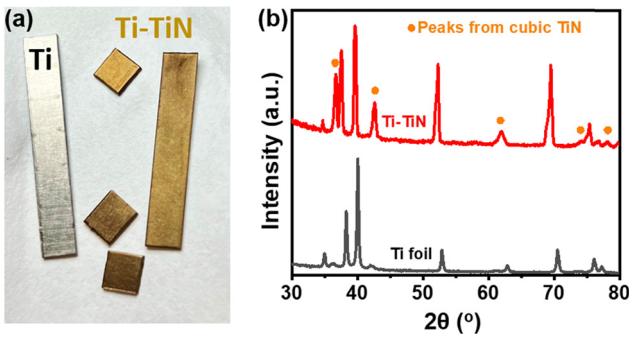

Fig. 1 (a) Colour optical photo of Ti–TiN and pristine Ti foil; (b) XRD patterns of Ti–TiN and pristine Ti foil. The peaks from cubic TiN are marked as orange dots in the XRD pattern of Ti–TiN.

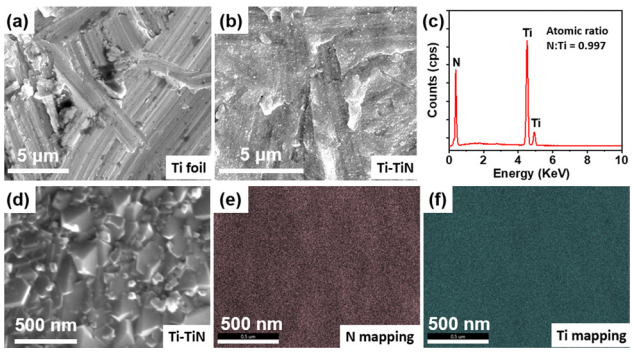

Fig. 2 (a) SEM image of pristine Ti foil; (b) SEM image of Ti–TiN; (c) EDX spectra of Ti–TiN from the region shown in (b) and (d) high-resolution SEM image of Ti–TiN; (e) EDX N mapping from the region shown in (d) and (f) EDX Ti mapping from the region shown in (d). All SEM images are secondary electron images.

Hall–Petch effect, which states that yield strength increases as grain size decreases. Energy dispersive X-ray (EDX) spectroscopy analysis provided quantitative information about the elemental composition of the cladding layer (Fig. 2c). The quantitative analysis yielded an atomic ratio of nitrogen to titanium of 0.99 ± 0.05, which is exceptionally close to the theoretical stoichiometric value of 1.0 for TiN. This near-perfect stoichiometry confirms the effectiveness of the $NaNH_2$-mediated nitriding process in achieving complete nitrogen incorporation. Trace element analysis revealed the absence of significant contamination from the molten salt medium or the reactor environment. Specifically, no detectable levels of chlorine, lithium, or potassium were observed in the nitride layer, confirming the effectiveness of the post-treatment cleaning procedures and the chemical inertness of the chloride salt system toward the titanium nitride product. Similarly, oxygen levels remained below the detection limit of the EDX system (approximately 0.5 at%), indicating successful exclusion of oxidizing species during the nitriding process. Fig. 2d and e present the results of EDX elemental mapping, showing the spatial distribution of titanium and nitrogen across the sample surface. Cross-section SEM analysis can provide critical information about the layer thickness and the interface characteristics between the nitride coating and the titanium substrate. As presented in Fig. 3a, although there are light and dark changes between the TiN crystal layer and the Ti substrate, there is no clear boundary, demonstrating the effectiveness of the molten salt medium in promoting uniform nitrogen diffusion and reaction. To measure the thickness of nitride layer, cross-section EDX line scan was performed. The compositional profiles (Fig. 3b) reveal the gradient element distribution through the nitride layer and into the underlying substrate and the nitrogen peak region around 1217 nm. Together, the morphological uniformity, conformal coating behaviour, and nanoscale grain refinement underscore the effectiveness of the molten salt nitriding approach in producing high-quality TiN coatings.

To shed light on the nitriding mechanism, a series of control experiments were conducted at different temperatures, with the resulting samples labeled as Ti–TiN-*x*, where *x* is the nitriding temperature in °C. As shown in Fig. S5 (ESI†), Ti–TiN-500 exhibited a light-yellow hue compared to pristine Ti foil, suggesting the formation of a thin TiN layer at just 500 °C. EDX analysis gave a N/Ti atomic ratio of ∼0.29; however, no nitride layer was detected by XRD or cross-section EDX line scan, indicating low crystallinity or insufficient thickness. At 700 °C, Ti_2N diffraction peaks appeared in XRD, and the N/Ti atomic ratio increased to ∼0.73. EDX line scanning revealed a nitrogen diffusion width of ∼1832 nm. At 800 °C, both Ti_2N and TiN phases were observed, with the N/Ti ratio reaching ∼0.94 and a reduced diffusion width of ∼1288 nm. At 900 °C, Ti–TiN displayed clear TiN peaks, a near-stoichiometric N/Ti ratio (∼1), and a diffusion width of ∼1217 nm. These results underscore the importance of high nitriding temperatures, specifically 900 °C to achieve a highly crystalline, stoichiometric TiN layer.

Nanoindentation tests provided quantitative assessment of the mechanical properties of the nitride layer, with particular emphasis on hardness enhancement compared to the untreated titanium substrate. Fig. 4a presents representative load-displacement curves obtained from nanoindentation tests performed on both the Ti–TiN specimen and the pristine Ti foil, revealing dramatic differences in mechanical response that reflect the successful formation of a hard nitride layer. The load-displacement curve for the Ti–TiN specimen exhibited a characteristic steep loading slope, reaching a maximum load of approximately 600 mN at a displacement of 2000 nm. This steep slope indicates high resistance to plastic deformation and is characteristic of hard ceramic materials such as titanium nitride. In contrast, the untreated titanium foil displayed a much more gradual loading curve with greater displacement at equivalent loads, reflecting the relatively soft and ductile nature of pure titanium. The unloading portions of the curves provided additional insights into the elastic-plastic behavior of the materials. The Ti–TiN specimen exhibited a relatively linear unloading curve with minimal hysteresis, indicating predominantly elastic recovery with limited plastic deformation. This behavior is consistent with the high elastic modulus and yield strength expected for titanium nitride. The untreated titanium showed more pronounced curvature in the unloading portion and greater hysteresis, reflecting the significant plastic deformation that occurred during loading. Quantitative analysis of the nanoindentation data using the Oliver-Pharr method yielded hardness values that demonstrated the exceptional effectiveness of the molten salt nitriding treatment (Fig. 4b). The nitrided Ti–TiN specimen achieved an average hardness of 20.6 ± 4.1 GPa, which corresponds to approximately 2100 HV when converted to the Vickers hardness scale using the relationship HV ≈ *H*/9.8, where *H* is the hardness in GPa.[26] This hardness value represents more than a four-fold increase

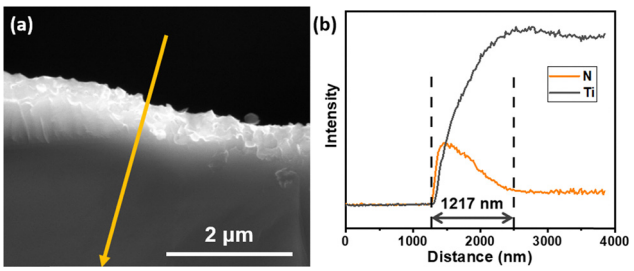

Fig. 3 (a) Cross-section SEM image of Ti–TiN foil; (b) EDX line scan curves for N and Ti corresponding to the orange arrow region in panel (a).

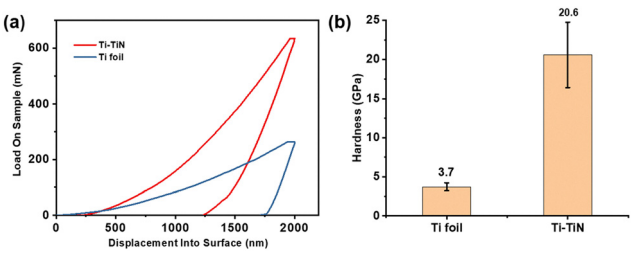

Fig. 4 (a) Loading–unloading curves of Ti–TiN and Ti foil in nanoindentation tests; (b) hardness comparison of Ti–TiN and Ti foil.

compared to the untreated titanium foil, which exhibited an average hardness of 4.8 ± 0.3 GPa (approximately 490 HV). Progressive scratch tests were performed to evaluate the interfacial bonding performance. As shown in Fig. S12 (ESI†), under a maximum applied load of 200 mN, the TiN layer exhibited localized fracture; however, no delamination from the Ti substrate was observed, demonstrating that the TiN coating possesses excellent adhesion to the Ti foil.

In conclusion, this work has successfully demonstrated that $NaNH_2$-mediated nitriding in molten salt systems represents a promising new approach for titanium surface modification with particular relevance to nuclear fuel cladding applications. The exceptional properties achieved, combined with the processing advantages, and improved safety characteristics, position this technique as a valuable addition to the surface modification toolkit for advanced materials applications.

This work was fully supported by the US Department of Energy (DOE) Office of Nuclear Energy under the Innovative Nuclear Materials program at Oak Ridge National Laboratory operated by UT-Battelle, under contract DE-AC05-00OR22725 with US DOE.

Conflicts of interest

There are no conflicts to declare.

Data availability

The data supporting this article have been included as part of the ESI.†

Notes and references

1 T. O. Igunma, A. T. Aderamo and O. H. Chukwuemeka, *Open Access Res. J. Eng. Technol.*, 2024, **7**, 16–30.
2 D. D. Keiser, *J. Nucl. Mater.*, 2019, **514**, 393–398.
3 C. Matthews, C. Unal, J. Galloway, D. D. Keiser Jr and S. L. Hayes, *Nucl. Technol.*, 2017, **198**, 231–259.
4 G. Jie, L. Shasha, R. Zhangshun, L. Jingjing, C. Dongyue, F. Xiaogang and L. Zhengcao, *Nucl. Eng. Des.*, 2024, **424**, 113208.
5 C. Matthews, U. Cetin, G. Jack and S. L. Hayes, *Nucl. Technol.*, 2017, **198**, 231–259.
6 F. G. Di Lemma, T. M. Trowbridge, L. Capriotti, J. M. Harp, M. T. Benson and R. D. Mariani, *J. Nucl. Mater.*, 2022, **558**, 153403.
7 I. Kim, F. Khatkhatay, L. Jiao, G. Swadener, J. I. Cole, J. Gan and H. Wang, *J. Nucl. Mater.*, 2012, **429**, 143–148.
8 F. Khatkhatay, J. Jian, L. Jiao, Q. Su, J. Gan, J. I. Cole and H. Wang, *J. Alloys Compd.*, 2013, **580**, 442–448.
9 F. Khatkhatay, L. Jiao, J. Jian, W. Zhang, Z. Jiao, J. Gan, H. Zhang, X. Zhang and H. Wang, *J. Nucl. Mater.*, 2014, **451**, 346–351.
10 I. Kim, L. Jiao, F. Khatkhatay, M. S. Martin, J. Lee, L. Shao, X. Zhang, J. G. Swadener, Y. Q. Wang, J. Gan, J. I. Cole and H. Wang, *J. Nucl. Mater.*, 2013, **441**, 47–53.
11 W.-J. Chou, G.-P. Yu and J.-H. Huang, *Surf. Coat. Technol.*, 2002, **149**, 7–13.
12 C. Li, D. Li, S. Zhang, L. Ma, L. Zhang, J. Zhang and C. Gong, *Nano-Micro Lett.*, 2024, **16**, 168.
13 T. Krekeler, S. S. Rout, G. V. Krishnamurthy, M. Störmer, M. Arya, A. Ganguly, D. S. Sutherland, S. I. Bozhevolnyi, M. Ritter and K. Pedersen, *Adv. Opt. Mater.*, 2021, **9**, 2100323.
14 K. Liang, A. Tabassum, A. Majed, C. Dun, F. Yang, J. Guo, K. Prenger, J. J. Urban and M. Naguib, *InfoMat*, 2021, **3**, 1422–1430.
15 Nitriding of titanium and titanium alloys, Total Materia, Total Materia Articles, 2024, **https://www.totalmateria.com/en-us/articles/nitriding-of-titanium-and-titanium-alloys/**.
16 M. Tarnowski, T. Borowski, S. Skrzypek, K. Kulikowski and T. Wierzchoń, *J. Alloys Compd.*, 2021, **864**, 158896.
17 A. M. Kamat, S. M. Copley, A. E. Segall and J. A. Todd, *Coatings*, 2019, **9**, 283.
18 N. Ohtsu, R. Endo, S. Takeda, K. Miura and K. Kobayashi, *Surf. Coat. Technol.*, 2022, **438**, 128362.
19 C. Zeng, H. Wen, A. H. Ettefagh, B. Zhang, J. Gao, A. Haghshenas, J. R. Raush and S. M. Guo, *Surf. Coat. Technol.*, 2020, **385**, 125397.
20 Y. Huang, Y. Gu, M. Zheng, Z. Xu, W. Zeng and Y. Liu, *Mater. Lett.*, 2007, **61**, 1056–1059.
21 H. Chen, C. Xiong, J. Moon, A. S. Ivanov, W. Lin, T. Wang, J. Fu, D.-E. Jiang, Z. Wu, Z. Yang and S. Dai, *J. Am. Chem. Soc.*, 2022, **144**, 10688–10693.
22 H. Chen, Z. Yang, Z. Zhang, Z. Chen, M. Chi, S. Wang, J. Fu and S. Dai, *Angew. Chem., Int. Ed.*, 2019, **58**, 10626.
23 V. T. Bonow, D. S. Maciel, N. L. Fenner, A. Reguly, A. Zimmer and C. G. Zimmer, *Clean. Eng. Technol.*, 2021, **4**, 100169.
24 G. Purwiandono, K. Manseki and T. Sugiura, *RSC Adv.*, 2020, **10**, 37576–37581.
25 D. Pye, *Practical nitriding and ferritic nitrocarburizing*, ASM international, 2003.
26 D. Tabor, *The Hardness of Metals*, Clarendon Press, 1951.

